High-Elevation Monsoon Precipitation Processes in the Central Andes of Peru

Steven Paul Chavez[1], Yamina Silva[2], and Ana P. Barros[1]

[1]Duke University
[2]Instituto Geofísico del Perú

November 26, 2022

Abstract

Measurements at the high-elevation Lamar Observatory in the Mantaro Valley in the Central Andes of Peru demonstrate a diurnal cycle of precipitation characterized by convective rainfall during the afternoon and nighttime stratiform rainfall with embedded convection. Based on 15 years of TRMM precipitation radar (PR) swath product 2A25, the area and rain type of precipitation features (PFs) over the Mantaro Valley showing PFs with areas smaller than 25,000 km and a mean daily ratio of convective to stratiform rainfall of 40/60. Data from three wet seasons 2016-2018 reveal long-duration (6-12 hours) precipitating systems (LDPS) that produce about 17% of monsoon rainfall for warming/cooling of Sea Surface Temperature (SST) in 2016/2018 during the El Niño/La Niña in the regions 3.4 and 1.2 of the Pacific. The LPDS fraction of monsoon rainfall doubles to 34% with weekly recurrence under warm and cool conditions in the region 1.2 and 3.4 respectively, that is the El Niño Costero. Backward trajectory analysis shows that precipitable water sustaining $> 80\%$ of seasonal precipitation and LPDS originate from the western Amazon. The analysis further shows that LDPS are associated with terrain-following moisture transport at low levels from the eastern foothills of the Andes under favorable weak South America Low Level Jet (SALLJ) conditions. LDPSs consist of late afternoon shallow embedded convection in the valley with trailing stratiform rainfall that persists until the early morning of the next day. The increase in the frequency of LDPSs explains the 30% increase in rainfall during 2017.

High-Elevation Monsoon Precipitation Processes in the Central Andes of Peru

S. P. Chavez[1,2], Y. Silva[2], and A. P. Barros[1]

[1]Duke University.

[2]Peruvian Geophysical Institute.

Corresponding author: Ana Barros (barros@duke.edu)

Key points:

- Monsoon precipitation consists of diurnal convection (>70%) and incidental stratiform long duration systems (LDPS)
- LDPS are tied to easterly moisture transport and terrain-following flow from the eastern Andes foothills at low levels
- Interplay of El Niño and South America Low Level Jet (SALLJ) governs inter-annual variability (~30% precipitation, #LDPS)

Abstract

Measurements at the high-elevation Lamar Observatory in the Mantaro Valley in the Central Andes of Peru demonstrate a diurnal cycle of precipitation characterized by convective rainfall during the afternoon and nighttime stratiform rainfall with embedded convection. Based on 15 years of TRMM precipitation radar (PR) swath product 2A25, the area and rain type of precipitation features (PFs) over the Mantaro Valley showing PFs with areas smaller than 25,000 km^2 and a mean daily ratio of convective to stratiform rainfall of 40/60. Data from three wet seasons 2016-2018 reveal long-duration (6-12 hours) precipitating systems (LDPS) that produce about 17% of monsoon rainfall for warming/cooling of Sea Surface Temperature (SST) in 2016/2018 during the El Niño/La Niña in the regions 3.4 and 1.2 of the Pacific. The LPDS fraction of monsoon rainfall doubles to 34% with weekly recurrence under warm and cool conditions in the region 1.2 and 3.4 respectively, that is the El Niño Costero. Backward trajectory analysis shows that precipitable water sustaining > 80% of seasonal precipitation and LPDS originate from the western Amazon. The analysis further shows that LDPS are associated with terrain-following moisture transport at low levels from the eastern foothills of the Andes under favorable weak South America Low Level Jet (SALLJ) conditions. LDPSs consist of late afternoon shallow embedded convection in the valley with trailing stratiform rainfall that persists until the early morning of the next day. The increase in the frequency of LDPSs explains the 30% increase in rainfall during 2017.

1 Introduction

Snow and rainfall in mountainous regions account for half the world's freshwater, their intensity, duration, and timing vary from one region to another, and in the same region, it is strongly modulated by elevation and landform (Barros, 2013). The Central Andes of Peru contains 70% of the world glaciers located in tropical latitudes (Chevallier et al., 2011) and their eastern slopes are considered an invaluable candidate for biodiversity conservation (Myers et al., 2000). However, it is a region with scarce weather and hydrological data (Peterson et al., 1997; Menne et al., 2012). Besides, most of the data such as precipitation measurements are available at daily time-scales and do not resolve the diurnal cycle, thus limiting the understanding of the current dynamics of precipitation in this region, let alone their sensitivity to future climate variability and change. Efforts to overcome these problems rely principally on using remote sensing measurements and simulations of climate models. However, these approaches require validation with in-situ observations. For example, in the foothills of the Central Andes of Peru TRMM product 3B42 underestimate annual rainfall up to 300% on average (Lowman & Barros, 2014).

The Central Andes of Peru encompasses mountain ridges above 6000 m ASL, canyons of 3000 m depth, myriad valleys, the Altiplano, and the Amazon rainforest at lower elevations. On the eastern slopes of the Peruvian Andes, in the Andes-Amazon transition, the low-level moisture flux coming from the Amazon is blocked by the mountains and turns southward out of the tropics of South America (Marengo et al., 2004; Vera et al., 2006). Enhanced convergence along the foothills of the Andes produces heavy rainfall, resulting in three hotspots of precipitation, i.e., regions where the mean annual rain is at least the double of the mean rainfall in the Amazon region (Espinoza et al., 2015; Chavez and Takahashi, 2017, hereafter CT17). Recently, a climatology of robust heavy orographic precipitation has also been linked to southerly cold fronts that originate in the mid-latitudes in South-America and latch to the eastern slope of the Andes in their northward progression (Eghdami and Barros, 2019). Besides, on the eastern slopes of the Andes, the complex and tortuous 3D topography results in strong precipitation gradients and complex spatial patterns of precipitation (Nesbitt and Anders, 2005; Biasutti et al., 2007; CT17).

The spatial distribution of precipitation is associated with favorable large-scale moisture transport and the interaction between precipitation systems and topography (Giovannettone and Barros, 2009; Romatschke and House, 2010). In the eastern foothills of the central Andes abundant moisture carried by the South American Low Level Jet (SALLJ) permit the development of mesoscale convective systems (MCSs) (Liu et al., 2011; Rassmussen et al., 2016; CT17), whereas dry conditions inhibit the MCSs' development at high elevations (above 3000 m ASL) (Moohr et al. 2014). However, valley systems' such as the Apurimac valley system (14ºS) channelize the moisture flux from the foothills of the Andes to the highlands (Killeen et al., 2007; Junquas et al., 2017). The reliability of the upslope moisture transport however is strongly tied to low-level entropy in the atmosphere, which in turn is closely tied to the modulation of atmospheric stability by evapotranspiration from montane forests (Sun and Barros, 2015).

According to the Tropical Rainfall measurement mission (TRMM) precipitation radar (PR) product 2A25 and the rain gauges form the Peruvian National Weather Service (SENAMHI) the rainiest region of Peru is located between Cusco and Madre de Dios (Nesbitt 2005, Biasutti,2007; Espinoza 2015, CT17). Most of the rainfall there is associated with large precipitation systems, 86% of these systems are associated with a stronger SALLJ, while the resting 14% are related to cold air incursions (CAIs) (CT17). An altitudinal transect of rain gauges, located slightly north of this precipitation hotspot, revealed that extreme rainfall is linked with CAIs which produce outstanding rainfall in the lower elevations and some important rainfall at higher elevations (Eghdami & Barros, 2019), the contribution from CAIs to rainfall in that region was estimated between 10-20 % (Eghdami, personal communication). During CAIs moisture transport at higher elevations is significantly larger (above 3500m) than days of normal and stronger SALLJ conditions (CT17; Eghdami & Barros, 2019). At the Quelccaya glacier, located next to the hot spot of precipitation, snow records show that cold air incursions are responsible of most of the snow accumulation (Hurley et al., 2015).

Solar forcing and local processes also influence the dynamics of precipitation. In the eastern slopes of the central Andes and at low elevations in the Apurimac valley system most of the rainfall is observed during the night and early morning (Giovannettone and Barros, 2009; CT17; Junquas et al., 2017). Nevertheless, in the highlands of the central Andes of Peru, most of the rainfall is observed in the afternoon (Mohr et al., 2014; CT17). High-resolution simulations of wind and the specific humidity in the Apurimac valley system (Junquas et al., 2017) show that daytime humidity is over the summits due to the local upslope valley winds while at night humidity is found in the valley associated with downslope flow. Indeed, using the TRMM precipitation features, Lowman and Barros (2014) showed that the centroids of precipitation features in the central Andes are in the ridges between 1-7 PM and in the Valleys between 1-7 AM.

Interannual variability of precipitation in the Peruvian Andes has long been linked to variability in ENSO activity. Takahashi et al. (2011) proposed two indices of Sea Surface Temperature (SST) tied to ENSO based on eastern Pacific (E) and central Pacific (C) conditions. Subsequent studies found that positive/negative C conditions are associated with dry/wet anomalies in the Central Andes of Peru, whereas positive E conditions are associated with the southern displacement of the Inter-Tropical Convergence Zone (ITCZ), and therefore more rainfall in northern Peru (Espinoza and Lavado, 2013; Sulca et al., 2018). Both indices are associated with westerly wind anomalies that generate less than average rainfall and negative mass balance in glaciers in the tropical Andes (Francou et al., 2004; Vuielle et al., 2008). However, the E index is more restricted to the southern part of Peru (Sulca et al., 2018). In 2016, 2017 and 2018, three different the El Niño flavors were identified: The central Pacific El Niño, the El Niño Costero (coastal) and the La Niña respectively. During the first months of 2016 the indexes 3.4, 1.2 and E and C identified a strong the El Niño, but was a dry year in Peru. During January-March of 2017 The El Niño Costero (coastal) that has only one reference back to 1925 (Takahashi & Martinez, 2019) developed rapidly in the region 1.2 with almost no warning, while been neutral in the region 3.4, which generated conflicting forecast reports from U.S and Peru (Ramírez & Briones, 2017). Opposite to the El Niño of the previous year, the El Niño Costero inundated the northern and central coast of Peru and generated landslides in the inter-Andean Valleys. In 2018, the indexes in regions 3.4 and 1.2 coincided that was a moderate the La Niña year (Fig. 11).

The meteorology of selected high-elevation monsoon rainfall in the central Andes has been studied previously at the event-scale (Moya et al., 2018; Flores-Rojas, 2019; Martinez-Castro et al., 2019). In this study, the primary objective is to characterize the diurnal cycle, vertical structure and microphysics of monsoon precipitation using observations in the Mantaro Valley (MV, Figure 1). MV is nestled in the central Andes with north-south orientation and mean elevation of 3300 m. MV's eastern (Amazonian) flank is the Huaytapallana chain that reaches 5500 m ASL elevation. The MV supplies the Capital of Peru Lima, where around 10 million people live, with food and hydroelectric energy, which could be negatively impacted by the recent acceleration of the Huaytapallana glacier retreat associated with global warming (e.g., Vuille et al. 2008; Rabatel et al. 2013) because this glacier is a key source of freshwater during the dry season. Furthermore, the MV is highly vulnerable to extreme hydrological events, including floods, frosts, and landslides (Lavado et al. 2010, Espinoza et al. 2013; Saavedra and Takahashi, 2017; Zubieta et al., 2016). Understanding the dynamics of precipitation in this valley has therefore high socio-economic value to local people as well as millions elsewhere who benefit from its resources.

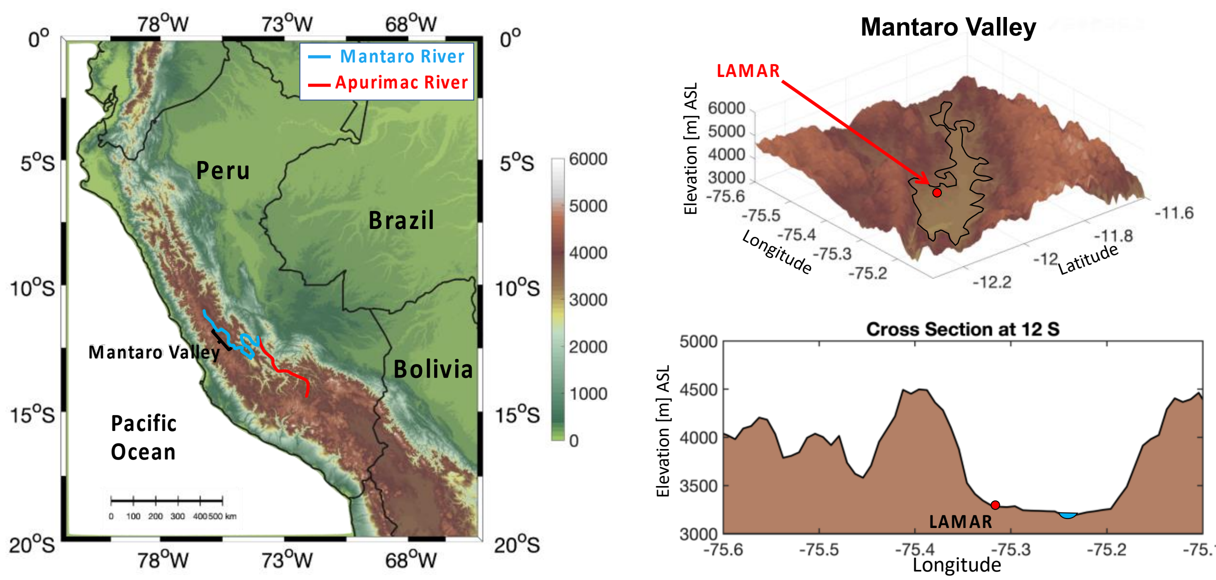

Figure 1- In the top a digital elevation model of the Central Andes of Peru. At the bottom, a 3D view showing a zoom of the Central Andes of Peru. The Mantaro Valley (MV) is the black area and the location of the Laboratory of Atmospheric Microphysics and Radiation LAMAR is the red dot.

The Laboratory of Atmospheric Microphysics and Radiation (LAMAR) of the Peruvian Geophysical Institute (IGP) is a measurement site that has been operational since 2015. LAMAR is equipped with a Ka-band vertical profiles radar, an optical disdrometer, two rain gauges, and a vertical profiler wind radar. These instruments measure for the first time in this region the vertical structure of precipitating systems, the rain type, the drop size distribution, and the low and mid-level winds. Finally, understanding regional precipitation processes including their vertical structure is critically important for satellite-based remote sensing of precipitation, in particular, to improve radar algorithms estimation of rainfall near the surface where ground-clutter in complex terrain introduces confounding ambiguity between stratiform and convective rainfall. The specific objectives of this study are: 1) to characterize the diurnal cycle and interannual variability of precipitation; 2) to characterize the drop size distribution associated with different types of precipitation observed at different hours of the day; 3) to determinate the diurnal variability of the echo-tops of precipitating systems between the Andes and the Amazon using the TRMM precipitation radar echo-top heights; 4) to use the continuous measurements of the ground Ka-band radar to identify and characterize the dominant precipitating systems, including their vertical structure; and 5) to map the relevant moisture source regions and examine the interannual variability of precipitation. In addition, a viability assessment of Global Precipitation Measurement Mission (GPM) observations over the region is conducted by examining GPM dual precipitation radar (DPR) and ground-based radar reflectivity profiles.

2 Data

Three monsoon seasons of reflectivity data from the Doppler pulsed 35 GHz Ka-band vertical profiler radar [January-March from 2016, December-March of 2017 and December-March of 2018] were used for analysis. Vertical profiles of wind velocity for each component *u*, *v* and *w* were obtained from the boundary layer tropospheric wind radar (BLTR) during January-March, 2016 and December-February, 2017. Rain gauge data at 1-minute temporal resolution from January 2016 to March 2018 were used to calculate rain rate and accumulation. Rainfall data between December of 2002 to January of 2017at a different site in the MV provides a long-term reference. Raindrop size spectra from an optical disdrometer Parsivel-2 were available from September, 2017 to March, 2018. In addition, 15 years of data (1998-2012) from the Tropical Rainfall Measurement Mission (TRMM) radar swath products 2A23 and 2A25 (Iguchi et al., 2000, 2009; Awaka et al., 2009; Kozu et al., 2009) were used to obtain precipitation features (PFs) and echo top heights. The Global Precipitation Mission (GPM) dual precipitation radar (DPR) Ku-band radar in normal scan (NS) mode was used to determinate the ground clutter free height. The Hysplit algorithm (Stein et al, 2015) was applied for backward trajectory analysis using as input Era-Interim Reanalysis meteorological data during each of three seasons January-March 2016-2018. Finally, data from Era5 Reanalysis was used to obtain the maps of Total Water Content (TWC) and to elaborate cross sections of the moisture flux components *uq* and *vq* during January and February of 2016-2018.

3 Methodology

Vertical reflectivity profiles from the Ka-band radar at the original temporal resolution of 5.3 s were averaged to 10 min. BLTR wind profiles were averaged to 10 min resolution as well. The diurnal cycle of reflectivity was obtained for rainy profiles considering only those reflectivity profiles where the near surface (280 m AGL) reflectivity is greater than 0 dB, which is an indicator that there is light rainfall in the surface as measured by the disdrometer and in situ observations. At the same time the profiles of each wind component were extracted to derive the diurnal cycle of every component of the wind when rains.

The horizontal extension and the rainfall produced by the precipitation features (PFs) over the Mantaro Valley in the 1998-2012 period were quantified from the TRMM2A25 swath product (Iguchi, 2000). The PFs are obtained from the instantaneous swaths and are defined as the rainy areas of contiguous pixels with estimated surface rain rate greater than 0.15 mm/h

(Romatschke and Houze, 2013). Convective and stratiform rainfall corresponding to each PFs exactly over the Mantaro valley was quantified from the classification of the TRMM 2A23 product (Awaka, 2009; Funk et al., 2013).

Transects of the echo-top height measurements of TRMM precipitation radar observations from the Andes to the Amazon were obtained following the methodology proposed by CT17 for the 1998-2012 period. These transects are centered in the topographic contour of 1000 m ASL and extend over the Andes-Amazon transition region along 10 - 13.5 S. The vertical distribution of echo-top heights was calculated by counting all echo-tops heights in bins of 200 m elevation for 6-hour intervals.

The diurnal cycle of the drop size distribution during the spring (SON) and summer (DJF) months was calculated based on the measurements of the drop size distribution from Parsivel-2 disdrometer. The vertical structure of the Ka-band reflectivity profiles for the 3 wet seasons 2016-2018 where summarized in a contour frequency by altitude diagram (CFAD) that displays the frequency distribution of radar reflectivity as function of height. The CFAD plot was constructed counting the reflectivity values observed for each bin of 31 m elevation and 1 dBZ considering a minimum threshold of -20 dBZ. In addition, the clutter free height was calculated for GPM DPR Ku NS in the period March 2014-March 2019 using as reference the GPM-DPR Level 2 algorithm theoretical basis document (Iguchi, 2018). A sample swath showing the clutter free height over the Central Andes is shown in Figure 7.

Precipitating systems (PSs) where identified in terms of their duration and vertical structure as they passed over the vertical profiling Ka-band radar during the 3 wet seasons 2016-2018. The PSs were extracted from the 10 min average reflectivity profiles time-series as follows. First, all the contiguous areas where reflectivity is higher than -15 dBZ are identified.

This low threshold accounts for radar attenuation and cloud regions reducing fragmentation of a single large precipitating system (PS), which is suitable for detecting embedded convection systems. Only the PSs that have at least one value of reflectivity higher than 20 dBZ near the surface were selected to eliminate cloud systems with no precipitation or very light precipitation. Next, the shape of each PS is quantified by fitting an ellipse to its area to determine the centroid of the ellipse and the minor and major axes, which are used as PS metrics. Because of the alignment of the PSs in the space of range and time, the major (vertical) axis gives information of PS range or height AGL and the minor (horizontal) axis represents the duration of the PS in minutes. Finally, the PSs were categorized as long-duration PS (LDPS) if they last 6 hours or more according to the Ka-band and rain gauge observations and No LDPS for all other PS lasting less than 6 hours. In addition, the diurnal cycle of cumulative hourly rainfall from the rain gauge corresponding to LDPS and No LDPS categories in January-February of 2016, 2017 and 2018 which are 3 very different years in terms of el Niño activity.

Moisture transport was analyzed from 48 hours wind back trajectories calculated by the HYSPLIT model (Stein et al, 2015) starting in the Mantaro Valley at 13 LT at 500 m above ground level. The trajectories were subset for days when nocturnal long duration and afternoon PSs were detected with no repeating days, i.e., if in the same day nocturnal and afternoon PS were detected we assign that day as a day with nocturnal PS and it does not count as a day with afternoon PS.

4 Discussion of Results

4.1 Vertical Profiles of radar reflectivity and winds when rains in LAMAR

The vertical profiles of reflectivity of precipitating systems (PSs) in the Mantaro Valley reveal a strong diurnal cycle (Fig 2) and the corresponding wind profiles provide insight into the underlying processes. In the afternoon, in particular between 16-20 LT the reflectivity profiles reach altitudes above 11 000 MSL, and vertical motion is upward in the lower 1 km, whereas it is downward or negligible at other times at all elevations. Both the rain and wind profiles are typical of deep convective activity in the afternoon (16-20 LT) as found in previous studies (Moya et al., 2018; Flores-Rojas, 2019; Martinez-Castro et al., 2019). During late night and early morning (20-07 LT), the reflectivity profiles show isolated peaks (bright-band effects associated with the ice-phase) below 5000 m ASL with concurrent changes in the downdrafts at that altitude associated with hydrometeor phase-change from solid to liquid which is typical of stratiform precipitation (Houze, 2014). However there are some intervals in early morning with no bright band and no downdrafts but instead updrafts winds, which are related to embedded convection associated to long duration PSs as seen in Fig 9. The mean zonal wind (Fig 2) is predominantly in the east-west direction prior to the onset of the maximum convective activity and weakens between 17-23 LT when convective activity is more intense. The mean meridional wind is in south-north direction except between 12-17 LT when it reverses direction.

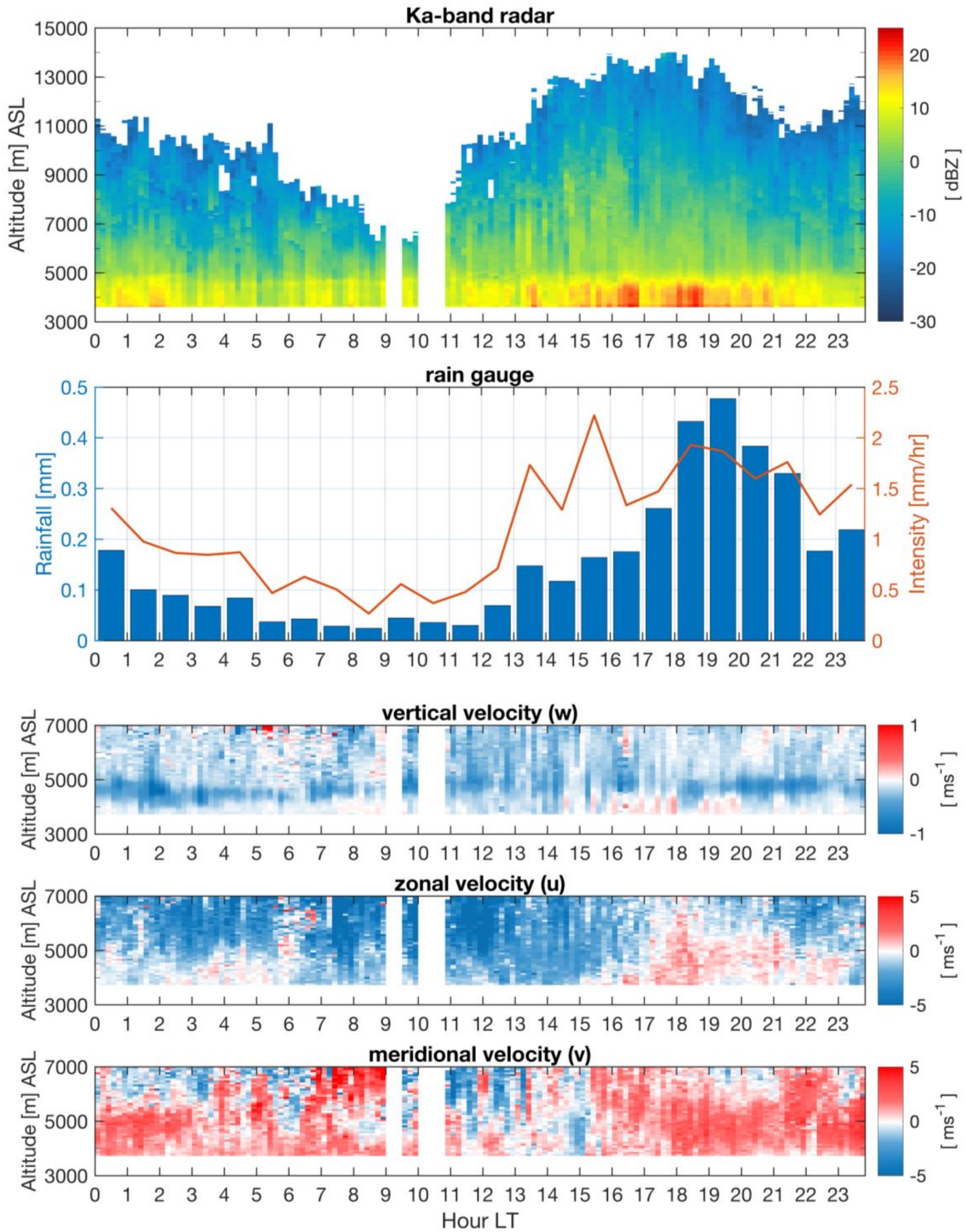

Figure 2- Diurnal cycle of reflectivity and winds vertical profiles when rains obtained from the Ka-band and the BLTR radar respectively during two wet seasons JFM of 2016 and DFJ of 2017 at the LAMAR site located in the Mantaro Valley (Fig 1). In addition, the mean hourly rain and rain rate from a rain gauge is shown as bars and an orange line respectively.

4.2 Precipitation systems over the Mantaro Valley

Following CT17, TRMM precipitation features (PFs) are categorized based on areal extent: Small (25- 2250 km2), Medium (2250 -24700 km^2) and Large (>24700 km^2) (Figure 3). The large PFs that contribute most of the rainfall in the eastern slopes of the Andes (CT17) are not observed in the high -elevations of the Mantaro Valley that is attributed to dry conditions that inhibit the development of large convective systems (Moohr et al., 2014). Based on the TRMM swath retrievals (Iguchi, 2000), the rain contribution in percentage to total rain over the Mantaro Valley of small PFs is 75% and medium PFs is 25%. By disaggregating the contribution to the total rain into intervals of 6 hours, it was found that afternoon (13-18 LT) small size PFs contribute 41 % of the TRMM daily rainfall based on 145 small size PFs and 10 medium size PFs in the record (Fig. 3). Indeed, the number of small size PFs is generally one order of magnitude higher than the number of medium size PFs. The rainfall contributions associated with convective and stratiform rain according to the TRMM PR 2A23 product classification (Awaka, 2009; Funk et al., 2013) are shown in black and white respectively (Fig 3). At daily scale, the principal contribution to the total TRMM rainfall in the Mantaro Valley comes from stratiform precipitation (60%). When disaggregating the rainfall contribution in intervals of 6 hours (Fig 3) the contribution of stratiform and convective rain remains around 60% and 40% respectively except during the early morning (01-06 LT) when the stratiform contribution is around 75%, and the convective contribution is 25%. Note that this classification misses shallow precipitation systems (Duan et al., 2015; Arulraj & Barros, 2019).

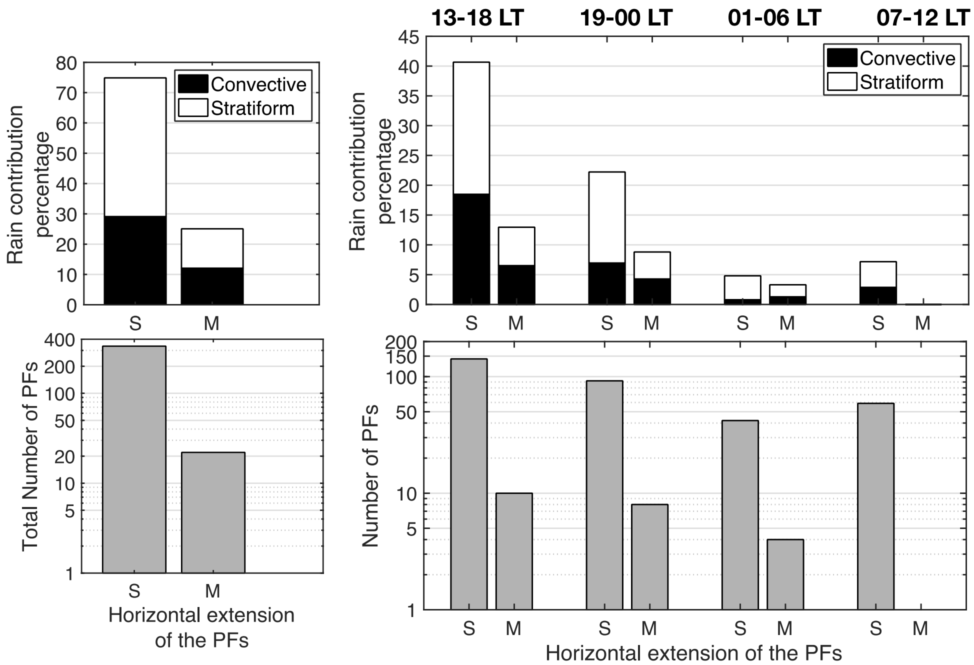

Figure 3- Contribution of small and medium size PFs to the rainfall in the Mantaro Valley during the wet season November-February (the contribution from convective and stratiform rainfall is shown in black and white respectively), and the number and the contribution of the small and medium size PFs to the total daily rainfall in percentage disaggregated in intervals of 6 hours.

4.3 Echo-top heights of the storms in the Andes and the Amazon transition

The distribution of echo-top height measurements along transects from the Andes to the Amazon (Fig. 4) between 10^{o}S and 13.5^{o} S reveals differences in the echo-top heights associated to the diurnal cycle of precipitating systems developed in the transition region from the Andes Mountains to the Amazon. In the context of Fig. 3, we consider the Andes Mountains as the region where the average terrain elevation is greater than 2000 MSL, and the Andes foothills the region where the average terrain elevation ranges between 500-2000 MSL. Higher echo-tops are observed in the mountains than in the foothills in the afternoon (13-18 LT). In the mountains (foothills) the echo-top heights range between 5000-13000 m (5000-9000m).

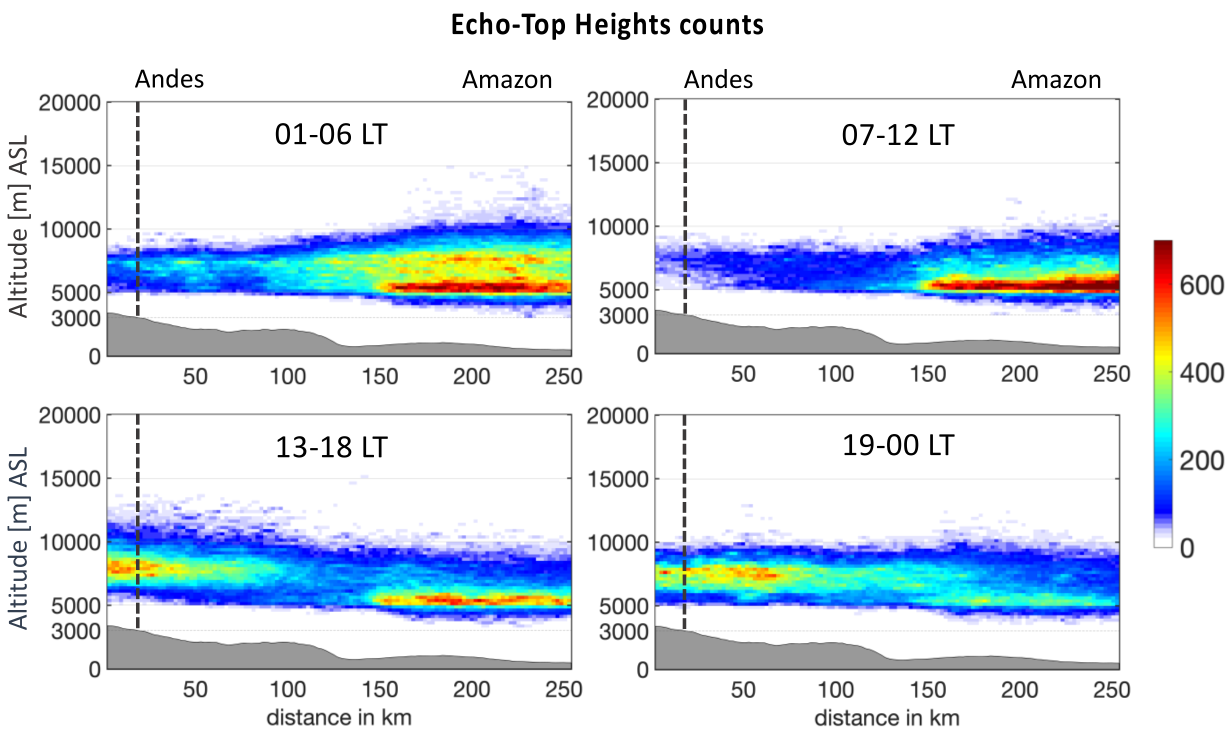

Figure 4- Echo-top heights counts in vertical bins of 200 m from TRMM precipitation radar along transects starting in the Andes and extended to the Amazon at intervals of six hours. The gray area is the terrain elevation of the mean of the transects. The transects latitudes ranges between 10 S and 13.5 S. The shading is the total count of echo-top heights for all the transects. The dashed line shown the location where the vertical pointing radar at LAMAR is located.

At LAMAR in particular (dashed-line in Fig. 4), the echo-top heights range from 5500 to 12,500 m, in agreement with measurements of the Ka-band radar (Fig. 2). In the evening and into mid-night (19-00 LT), the number of echo-top heights between 5,000-9000m diminishes in the foothills, and the echo-tops above 10,000m are not observed in the mountains. At that time, the echo-top heights range from 5,000-10,000 m at LAMAR. In the early morning (01-06 LT), higher echo-tops heights are observed in the foothills than in the mountains, reaching the daily maximum altitude as in CT17 who showed that greater depth and higher rain rate of convective systems in the Andes-Amazon transition region are observed at that time. Mountain downslope winds from the Andes mountains converging with the moist flow from the Amazon basin might be present along the Andes foothills as suggested by Giovannettone and Barros (2009). At the location of LAMAR, the echo-top heights range from 5,000-8,000 m, which is also in agreement with measurements of the Ka-Band radar. Fewer echo-tops are observed in the Andes and in the foothills in the morning (7-12 LT) with more towards the Amazon compared to the previous hours. Precipitating systems, at that time, are decaying from more convective to more stratiform rain (CT17).

4.4 Diurnal cycle of the Drop Size Distribution (DSD)

Measurements of the DSD from an optical disdrometer for the spring season September-November of 2017 and summer corresponding to January-March 2018 were averaged per hour and the diurnal cycle (Fig. 5) was analyzed separately.

In the spring season, large drops with diameters greater than 1.75 mm are observed only in the afternoon (15-21 LT); these drops can reach diameters of 3 mm as expected of convective rainfall. During the late night and early morning (22-07 LT), number drop concentrations arever low for diameters under 1 mm. Around midday a great concentration of small hydrometeors with diameters less than 0.5 mm could to be related to orographic enhancement via low-level Seeder-Feeder Interactions as observed in the southern Appalachians (Wilson & Barros, 2014; Duan and Barros, 2017) though additional measurements would be necessary to be conclusive.

In the summer months, i.e. January-March of 2018, large number concentrations are observed at all times compared to the spring, except around noon. Large drops with diameters greater than 1.75 mm are observed between 15-21 LT and in early morning 2-6 LT. The presence of large drops in early morning is associated with the peak in rainfall produced by LDPSs at that time (Fig. 12). Indeed, a moderate La Niña was detected in the Pacific region 3.4 in the summer of 2018 which previous studies (Lavado and Espinoza, 2013) relate to increase of rainfall in the central Andes of Peru at LAMAR location (The vertical reflectivity profiles for the summer of

2018 also show reflectivity values reaching higher elevations in early morning compared to the previous year (Fig. S1).

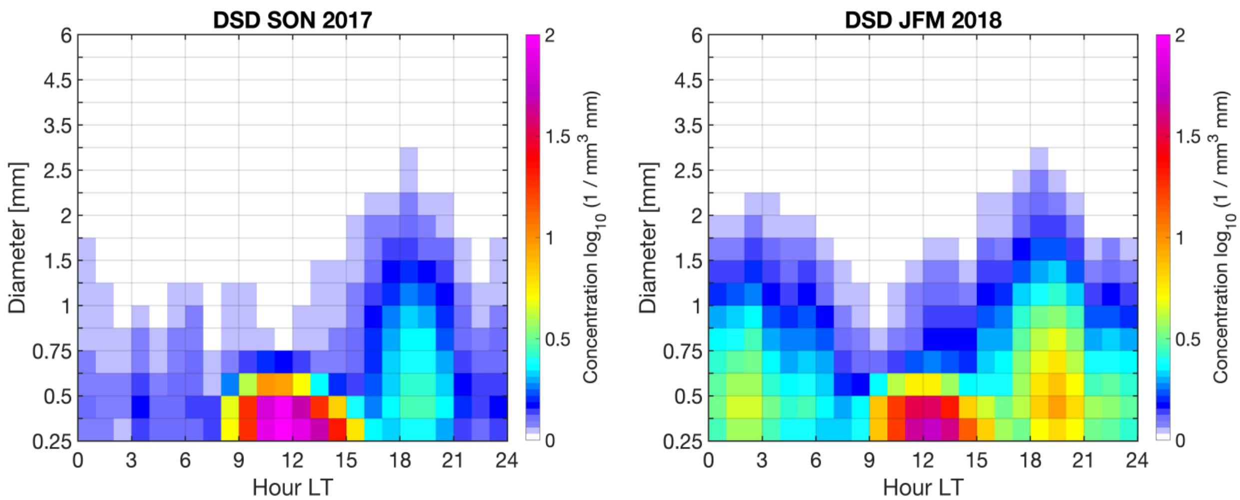

Figure 5- Diurnal cycle of the drop size distribution from measurements of the optical disdrometer Parsivel2 corresponding to September-November of 2017 and January-March 2018. The x-axis are the hours of the day, the y-axis is the diameter of the hydrometeors and in shading the concentration.

4.5 Vertical profiles of reflectivity from the ground Ka-Band and GPM Ku band.

The vertical structure of the Ka-band reflectivity profiles is depicted in Fig. 6 for the 2016, 2017 and 2018 wet seasons. On average the 0^o isotherm is at 5,000 m ASL or 1,700 m AGL, and it is associated with hydrometeors' phase change from solid to liquid that produces a bright-band (local reflectivity peak). The mean vertical structure reveals higher reflectivity values below the isotherm of zero degrees, located between 4900-5100 m ASL or 1600-1800 m AGL.

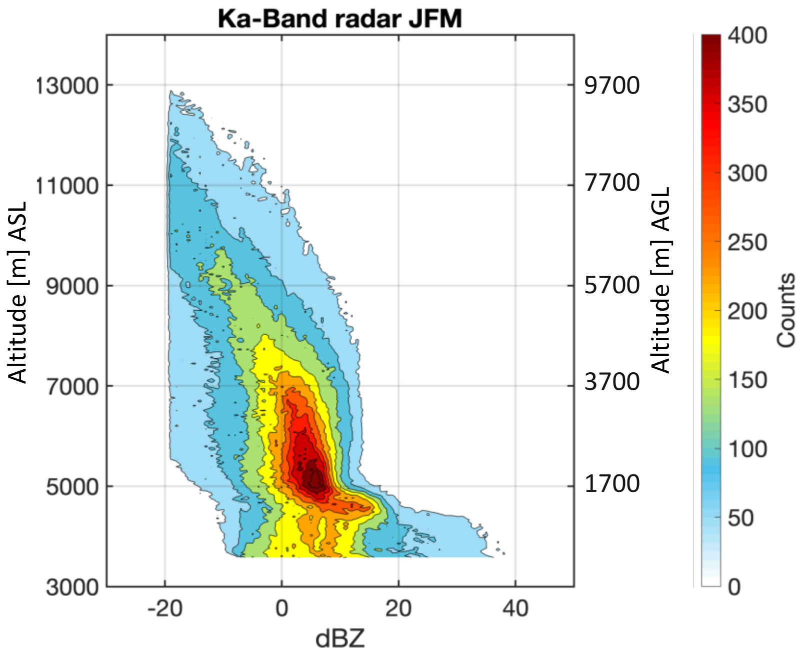

Figure 6 - CFAD for 3 wet seasons, i.e., JFM months of 2016-2018. The shading is the number of counts in bins of 31m altitude and 1dBZ resolution.

Figure 7 shows the height (blue line) of the clutter free region for the GPM-DPR Ku band for one randomly selected overpass among all examined. In the example, the blue line is above the 0^{o} isotherm indicating that shallow precipitation systems cannot be detected. Arulraj and Barros (2019) showed that contamination of near-surface reflectivity profiles due to ground-clutter is the major source of error in the Ku-PR quantitative rainfall estimates in the Southern Appalachian Mountains, and that the contaminated region can extend from 1.5 km to 3 km above ground level depending on the radar view angle (AGL). In the Mantaro Valley, during the lifetime of GPM DPR (2014-2019) the height of the ground-clutter region ranges between 0.9 km to 2.1 km AGL, having an average of 1.5 km AGL. Due to the elevated topography (3300 m ASL), the height of the contaminated region is 44% / 56% of the time above/below the 0^{o} isotherm, which suggests large underestimation of rainfall in this region.

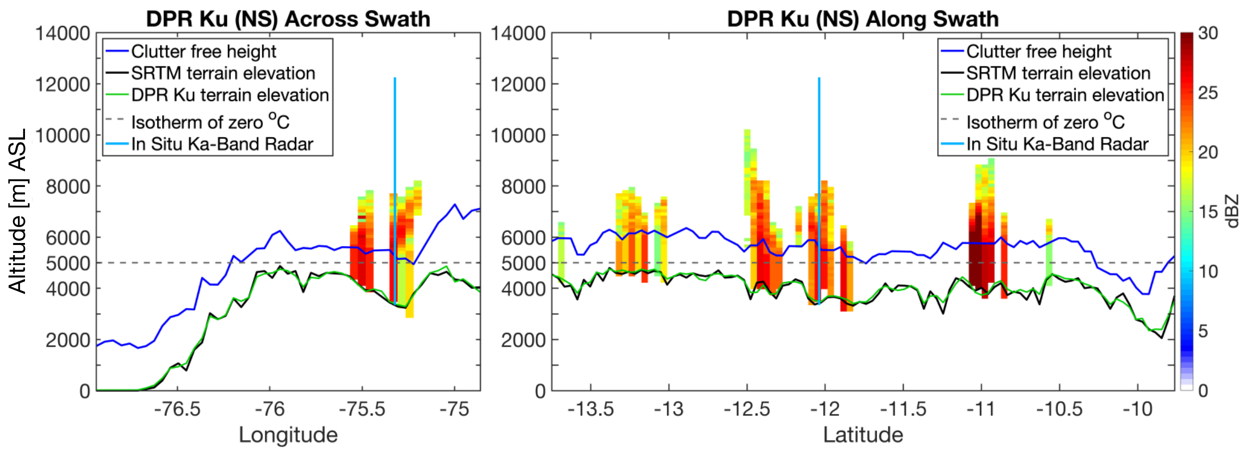

Figure 7- GPM DPR Ku NS cross sections of reflectivity across the swath and along the swath.

4.6 Long duration nocturnal and afternoon precipitating systems

The focus in this Section is on PSs obtained from the Ka-band radar continuous measurements. As a PS passes over the radar, the radar captures its vertical structure and duration. The reader should note that the PSs are different from the precipitation features (PFs) obtained from the instantaneous TRMM swaths: PSs are obtained from time continuous ground-based radar measurements; and the PFs are snapshots of the rainy area from the satellite.

A total of 11 LDPSs were observed by the Ka-band radar during three wet seasons corresponding to January and February of 2016, 2017, and 2018. Most of these long duration systems start in the late afternoon and persist until dawn (06 LT) (Fig. 11). In terms of frequency, during JF of 2016, 2 LDPS contribute 17% of rainfall, in JF of 2017, 7 LDPS events contribute with 35% of rainfall, and during JF of 2018, 2 events contribute with 17% of rainfall.

The mean vertical structure of PSs at different hours during the day is shown alongside that of nocturnal LDPSs in Fig. 8. PSs were assigned to the time interval where they spend more time. The Ka-band radar detects not only the precipitating regions but also the cloud structure; therefore, Fig 8 shows that the full development of some PSs can reach altitudes 12000 m ASL or 8700 m AGL. In addition, figure 8 shows that the probability density function of the radar echo heights corresponding to the nocturnal LDPSs is more similar to the afternoon PSs (15-20 LT) than to other nighttime PSs. Examples of afternoon and nocturnal PSs and their drop size distributions (Fig. 9) show some common features, such as embedded convection, the presence of a bright band and large drops > 2mm.

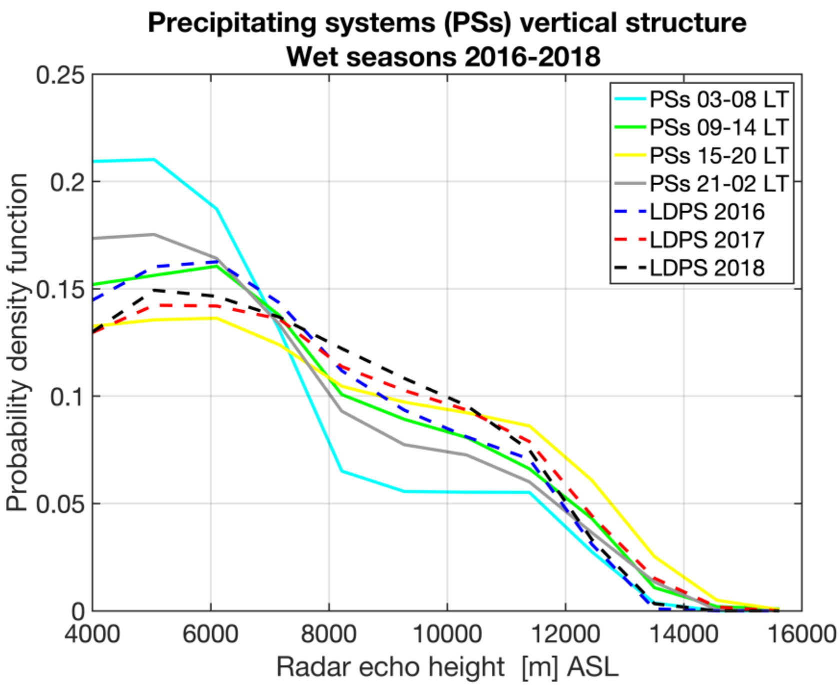

Figure 8- Probability density function of the Ka-band radar echo heights of precipitating systems (PSs) observed at different hours and specifically for nocturnal long duration PS (LDPS) for different years.

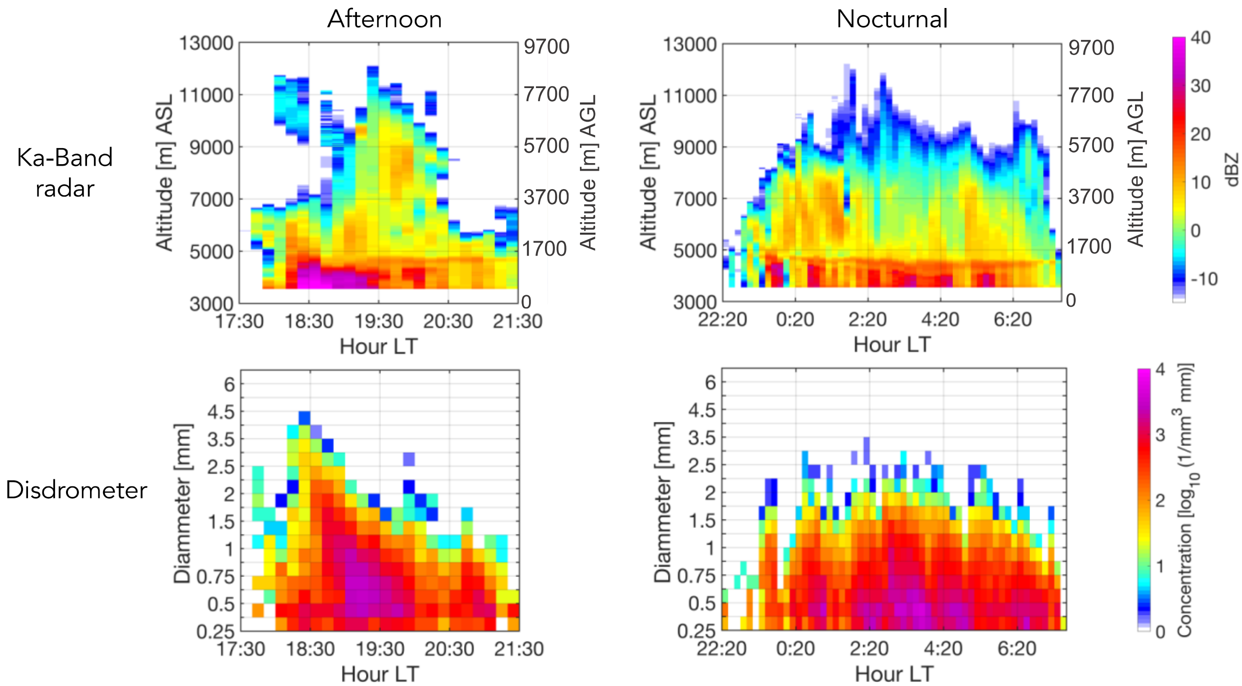

Figure 9- Ka-band reflectivity vertical profiles and disdrometer raindrops diameter concentration measurements for two PSs one during the afternoon and the other at nightime.

Backward trajectories for nocturnal long duration and afternoon short duration PSs show that the principal moisture source is the low-level moisture convergence zone along the eastern Andes foothills (Fig 10; see also Sun and Barros, 2015). Moist air reaching the LAMAR site at 13 LT comes from adjacent ridges (02-13 LT) which in turn can be traced successively to upwind valleys and ridges all the way down to the foothills over a two-day period with solar forcing driving upslope (daytime) and downslope (nighttime) winds over the landform. Except for one case, the remote easterly moisture transport linked to the long duration nocturnal PSs contribute with 25% of the rainfall during January and February of 2016-2018. Moisture source regions for the afternoon short duration afternoon events are at high elevations in the Western Cordillera and along the valley from the northwest as found in previous studies (Moya et al., 2018; Flores-Rojas, 2019; Martinez-Castro et al., 2019). In general, for the 3 wet seasons 2016-2018 the trajectories coming from the western Cordillera and from the eastern slopes of the Andes account for 10% and 75 % of the total seasonal rainfall respectively, the remainder 15% of seasonal rainfall correspond to nocturnal short duration PSs.

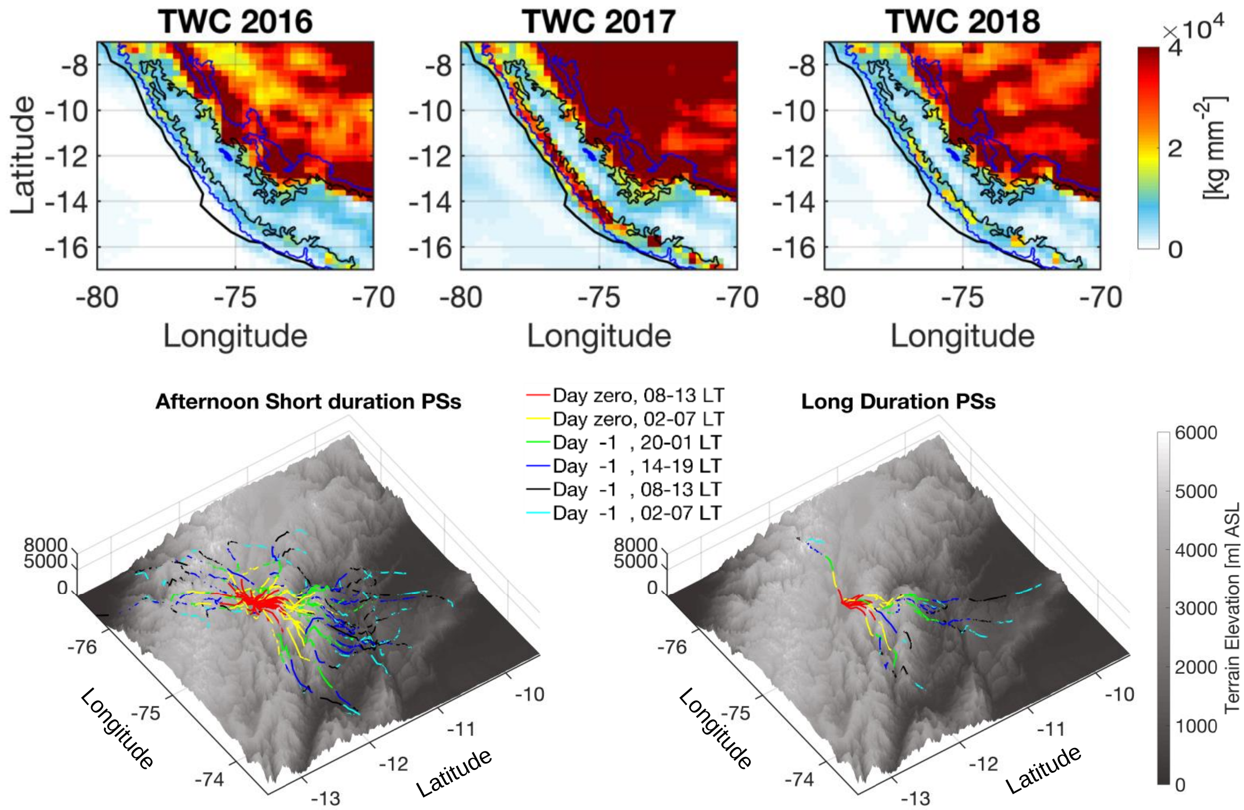

Figure 10- Top: Total Water Content during January and February from ERA 5 reanalysis. Bottom: Temporal evolution of HYSPLIT trajectories that start at 13 LT in the Mantaro Valley, for days when afternoon short duration and long duration precipitating systems were identified in January and February 2016-2018.

Back Trajectories and Interannual Variability

Moisture transport from the eastern foothills of the Andes to Mantaro Valley (MV) associated with No LDPS, i.e. PS lasting less than 6 hours, was mainly tracked to the eastern foothills of the Andes, and specially for LDPS, 10 of 11 associated back trajectories originate at the eastern foothills of the Andes. Over a two-day period, low level moisture associated with LPDS moves from the eastern foothills along the orographic envelope of the eastern Andes to reach the MV

(Fig.10). In this section, we examine the inter-annual variability of LDPS activity in the context of key elements of regional hydrometeorology: ENSO conditions over the Pacific and moisture convergence along the Andes foothills that is related to changes in the strength of the South American Low-Level Jet (SALLJ). East of the MV the SALLJ direction is from north west to south east i.e. almost parallel to the topography. Figure 11 shows cross-sections at 12^{o}S latitude show the East-West moisture flux component *uq* at 13 LT (1PM) in January of 2016, 2017 and 2018, this component is positive (to the east) at low elevations east of the MV every year and negative (to the west) at some altitudes above 4000m when the SALLJ is weaker. A month-by-month detailed analysis can be found in Supplemental Information (Fig. S2). The SALLJ intensity changes from year to year but also from month to month. In January 2016, the SALLJ was strong and the strongest in the four-year period analyzed here. Thus, less moisture reaches the Andes and no LDPS were detected in the MV. In February of the same year the SALLJ weakened and 2 LDPS were detected in the MV; the back trajectories for these 2 days originate in the eastern foothills, and the total amount of rainfall measured in January and February of 2016 was 200 mm. In addition, 2016 was considered a strong El Niño in region 3.4 and the ONI index in JFM was 2.2. In January of 2017, the SALLJ was the weakest with strong moisture flux toward the Andes between 4000-6000 m (Fig. 12). These favorable conditions were associated with the detection of 5 LDPS in the MV, four of which can be traced to eastern foothills and one at the western Andes Cordillera. Although the SALLJ strengthened in February of 2017 at lower levels, moisture transport to the west in the mid-troposphere at altitudes between 4000-6000 m remains strong. Rainfall in the MV for January and February was 313 mm, 35 % of which is associated with the LDPSs and explains 2/3 of the rainfall accumulation difference between 2016 and 2017. The Oceanic Niño Index (ONI) index was neutral in 2017, but the Sea Surface

Temperature (SST) anomalies in the region 1.2 are large consistent with El Niño Costero (Table 1). In January of 2018, the SALLJ was stronger than in January of 2017 but weaker than January of 2016, and 2 LDPS were detected in the MV linked to the eastern foothills. In February of 2018 the SALLJ was even weaker than in January and no LDPS were detected in the MV. In JFM of 2018 the ONI index, and the anomalies in the regions 1.2 and 3.4 indicate La Niña conditions (Table 1). Despite La Niña conditions, the total accumulation in January and February of 2018 was a modest 238 mm due to strong SALLJ activity. This analysis suggests that inter-annual variability of monsoon precipitation in the High-Andes is governed by teleconnections to Niño activity in the Pacific and synoptic-scale circulation in the Amazon to the west which affect the diurnal cycle and in particular the intra-seasonal frequency of LDPS.

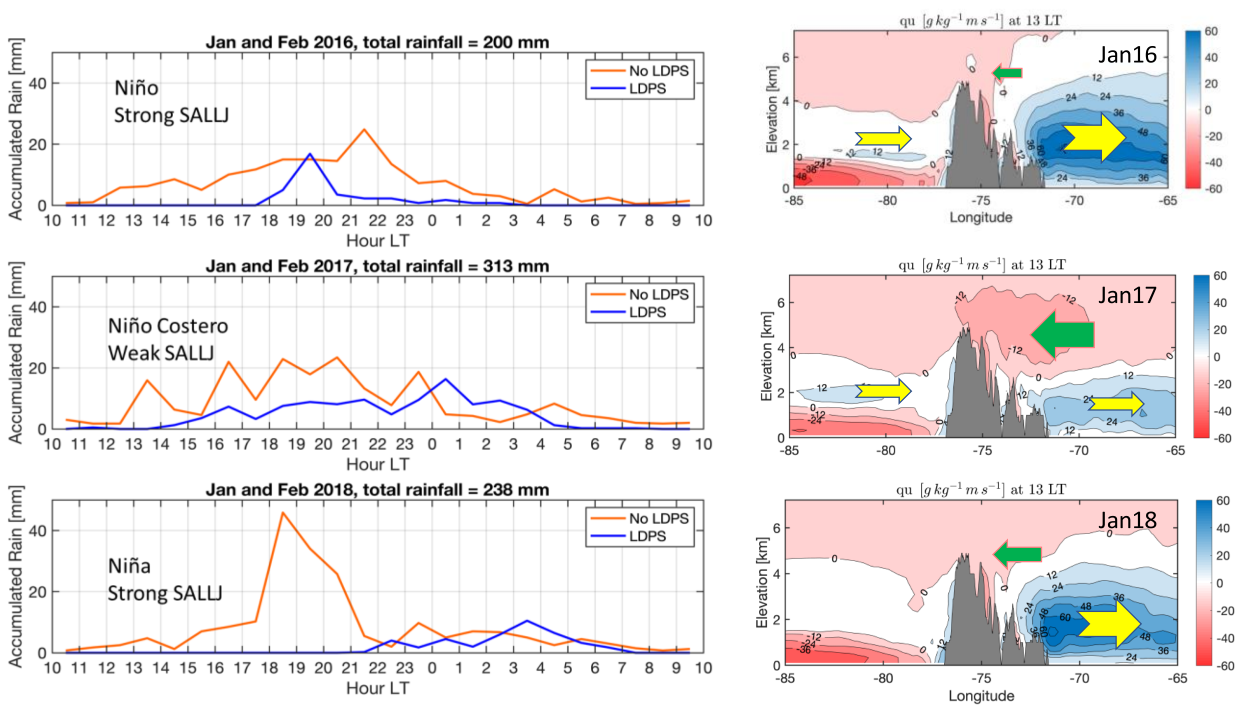

Figure 11- Left: Accumulated rainfall during January and February for years 2016-2018 at different hours. The rainfall from LDPS is the blue line and rainfall from No LDPS (i.e., PS lasting less than 6 horus) is the orange line. Right: Cross section at 12 S of the East-West component of the moisture flux *uq* at 13 LT for January of 2016-2018. The arrows represent the

direction to the east (yellow) and to the west (green) of *uq*, the size of the arrow represent the magnitude.

Year	Month	E	C	Region 1.2	Region 3	ONI JFM	Rain [mm] Mantaro Valley
2016	1	1.87	1.93	1.81	2.59	2.2	200
2016	2	1.18	1.95	1.38	1.97		
2017	1	0.44	-0.79	0.95	-0.08	-0.1	313
2017	2	0.79	-0.70	1.44	0.42		
2018	1	-1.04	-1.18	-1.10	-1.19	-0.8	238
2018	2	-0.91	-0.98	-0.89	-0.91		

Table 1- The table shows the most common ENSO indexes, which correspond to different locations and time scales. The last column shows the accumulated rainfall from January and February measured in the Mantaro Valley.

5 Conclusions

The diurnal cycle of precipitation in the central Andes of Peru characterized by nocturnal and early morning stratiform and afternoon convective precipitation was revealed by the TRMM precipitation radar (PR), in-situ radars, rain gauges and an optical disdrometer.

TRMM PR echo top heights were used with the idea of extending the observations of the vertical structure of storms to the surrounding of the Mantaro Valley. In particular, the top of the vertical profiles of reflectivity when rain is observed at LAMAR is in agreement with the TRMM PR measurements of echo-top heights.

The diurnal cycle shows during 15-20 LT convective activity with vertical profiles reaching 13000 m ASL, vertical wind updrafts, maximum rain and rain rate (Fig 2) and large drops (Fig 5). In addition, between 13-18 LT the echo-top heights are higher in the Andes mountains than in the Andes foothills (Fig 4). During late night and early morning 20-06 LT, a bright band and vertical downward winds suggest stratiform precipitation. Furthermore, at that time the echo-top heights in the Andes mountains reach lower altitudes than in the afternoon and are lower than the echo-top heights at the Andes foothills. However, the rain rate is significant, and some large drops are measured (Fig 5).

The spatial structure of the precipitation systems that affect the Mantaro Valley was characterized by synthesizing 5 years of TRMM PR observations and shows that precipitation is produced by precipitation systems (PFs) of small and medium size in contrast with large PFs like in the Andes foothills (Chavez & Takahashi, 2017). In the afternoon (12-18 LT) around 40 % of the daily rainfall is produced by small size PFs, and the ratio between convective and stratiform rain is 45/55. During the night (19-00 LT) the ratio of stratiform over convective precipitation is higher, and in the early morning the rainfall is principally stratiform. According to the TRMM PR, 60% of daily rainfall is stratiform and and 40% is convective. Despite agreement with previous global studies (Funk et al., 2013), these values are strongly influenced by the clutter free height (1-3 km) demonstrated here for the GPM DPR that results in large missed detection rates and underestimation of shallow precipitation systems overall. Furthermore, if the 0^o isotherm is below the clutter-free height, the algorithms that rely on the presence of a bright band to classify precipitation as stratiform fail as it cannot be detected (Awaka et al., 2009).

LDPS consist of afternoon shallow embedded convection in the valley with nighttime stratiform rainfall that often extend until the early morning of the next day is remarkable that only 11 long duration nocturnal precipitation systems (PSs) contribute around 25% of the rainfall during 3 wet seasons 2016-2018. LDPSs are important in terms of sustained soil saturation with potential to trigger landslides (Tao and Barros, 2014).

Wind back trajectories show that the air reaching the Mantaro Valley, the days when long duration nocturnal and afternoon PSs were observed, came mainly from eastern slopes of the

Andes and follows a trajectory composed of one after other solar driven mountain-valley breezes.

East of the MV the SALLJ direction is from north west to south east. The East-West moisture flux component *uq* in January-February of 2016, 2017 and 2018 is to the east at low elevations east of the MV every year and to the west at altitudes above 4000m when the SALLJ is weaker. As stronger the SALLJ more moisture is transported away from the Andes towards the Amazon. In El Niño year (2016) when the SALLJ was stronger in the period 2016-2018 less moisture reaches the Andes. Thus, less rainfall and only 2 LDPS were detected in the Mantaro Valley. On the other hand, when the SALLJ weakens, such as in the El Nino Costero (2017) and La Nina (2018) years, more total rainfall associated with an increase number of LDPS is observed in the Mantaro Valley.

The Mantaro Valley elevation is a significant challenge for GPM DPR Ku-band, the height of clutter-free ranges between 900-2100 m ASL, and 44% of the time is above the isotherm of zero degrees (5000 m ASL). Therefore GPM DRP Ku-band does not capture the processes occurring close to the surface and according to the in-situ Ka-band radar, reflectivity increases towards the surface (Fig 10). Detection and underestimation errors tied to ground clutter artifacts should be especially important in the case of LDPS, which in turn should result in large-interannual variability in the uncertainty of satellite-based precipitation.

Acknowledgments

Thanks to NASA for the TRMM precipitation radar data, the data used in this effort were acquired as part of the activities of NASA’s Science Mission Directorate and are archived and distributed by the Goddard Earth Sciences (GES) Data and Information Services Center (DISC).

The authors gratefully acknowledge the NOAA Air Resources Laboratory (ARL) for the provision of the HYSPLIT transport and dispersion model and/or READY website (http://www.ready.noaa.gov) used in this publication.

The second author was supported by the project "Study of the physical processes that control the superficial flows of energy and water for the model of frost, intense rains, and evapotranspiration in the central Andes of Peru" financed by Innovate Peru (Contract Nº 400-PNICP-PIBA-2014).

We are grateful to Dr. Danny Scipion by his help in processing the wind radar data and the team of the Huancayo observatory and LAMAR laboratory from the Instituto Geofísico del Perú (IGP), who bring support and maintenance to the radars and instruments.

References

Arulraj, M., & Barros, A. P. (2019). Improving quantitative precipitation estimates in mountainous regions by modelling low-level seeder-feeder interactions constrained by Global Precipitation Measurement Dual-frequency Precipitation Radar measurements. *Remote Sensing of Environment*, *231*, 111213.

Awaka, J., Iguchi, T., & Okamoto, K. I. (2009). TRMM PR standard algorithm 2A23 and its performance on bright band detection. *Journal of the Meteorological Society of Japan. Ser. II*, *87*, 31-52.

Barros, A. P. (2013). "Orographic precipitation, freshwater resources, and climate vulnerabilities in mountainous regions," in Climate Vulnerability: Understanding and Addressing Threats to Essential Resources, Vol. 1, eds J. Adegoke and C. Y. Wright (Waltham, MA: Elsevier Inc.; Academic Press), 57–78. doi: 10.1016/B978-0-12-384703-4.00504-9

Biasutti, M., S. E. Yuter, C. D. Burleyson, and A. H. Sobel (2012), Very high resolution rainfall patterns measured by TRMM precipitation radar: seasonal and diurnal cycles, Clim. Dyn., 39(12), 239–258.

Chavez SP, Takahashi K (2017) Orographic rainfall hotspots in the Andes–Amazon transition according to the TRMM precipitation radar and in situ data. Geophys Res Atmos. doi:10.1002/2016JD026282

Chevallier, P., Pouyaud, B., Suarez, W. et al. Reg Environ Change (2011) 11(Suppl 1): 179. https://doi-org.proxy.lib.duke.edu/10.1007/s10113-010-0177-6

Egger, J., and Coauthors, 2005: Diurnal circulation of the Bolivian Altiplano. Part I: Observations. Mon. Wea. Rev., 133, 911– 924.

Espinoza, J. C., S. Chavez, J. Ronchail, C. Junquas, K. Takahashi, and W. Lavado (2015), Rainfall hotspots over the southern tropical Andes: Spatial distribution, rainfall intensity, and relations with large-scale atmospheric circulation, Water Resour. Res., 51, 3459–3475, doi:10.1002/2014WR016273.

Espinoza, J. C., J. Ronchail, M. Lengaigne, N. Quispe, Y. Silva, M. L. Bettolli, G. Avalos, and A. Llacza (2013), Revisiting wintertime cold air intrusions at the east of the Andes: Propagating features from subtropical Argentina to Peruvian Amazon and relationship with large-scale circulation patterns, Clim. Dyn., 41(7–8), 1983–2002.

Falvey, M., & Garreaud, R. D. (2005). Moisture variability over the South American Altiplano during the South American Low Level Jet Experiment (SALLJEX) observing season. Journal of Geophysical Research, 110(D22), D22105–12. http://doi.org/10.1029/2005JD006152

Flores Rojas, J. L., Moya-Álvarez, A. S., Kumar, S., Martínez-Castro, D., Puma, V., Edmundo, E., & Silva Vidal, Y. (2019). Analysis of Possible Triggering Mechanisms of Severe Thunderstorms in the Tropical Central Andes of Peru, Mantaro Valley.

Francou B, Vuille M, Favier V, Cáceres B. 2004. New evidence for an ENSO impact on low latitude glaciers: Antizana 15, Andes of Ecuador, 0°28'S. *J. Geophys. Res.* **109**: D18106. https://doi.org/10 .1029/2003JD004484.

Funk, A., Schumacher, C., & Awaka, J. (2013). Analysis of rain classifications over the tropics by version 7 of the TRMM PR 2A23 algorithm. *Journal of the Meteorological Society of Japan. Ser. II*, *91*(3), 257-272.

Giovannettone, J., and A. Barros (2009), Probing regional orographic controls of precipitation and cloudiness in the central Andes using satellite data, J. Hydrometeorol., 10(1), 167–182.

Iguchi, T., Meneghini, R., Awaka, J., Kozu, T., & Okamoto, K. (2000). Rain profiling algorithm for TRMM precipitation radar data. *Advances in Space Research*, *25*(5), 973-976.

Iguchi, T., Seto, S., Meneghini, R., Yoshida, N., Awaka, J., Le, M., Chandrasekar, V., Brodzik, S. & Kubota, T. (2018). GPM/DPR Level-2 algorithm theoretical basis document. NASA/ JAXA Tech. Rep. Retrieved from: https://pps.gsfc.nasa.gov/Documents/ATBD_DPR_201811_with_Appendix3b.pdf

Junquas C., Takahashi K., Condom T., Espinoza JC., Chavez, S., Sicart JE, Lebel T., 2017: Understanding the influence of orography over the precipitation diurnal cycle and the associated atmospheric processes in the central Andes. Climate Dynamics. DOI 10.1007/s00382-017-3858-8.

Killeen, T. J., M. Douglas, T. Consiglio, P. M. Jørgensen, and J. Mejia (2007), Dry spots and wet spots in the Andean hotspot, J. Biogeogr., 34(8), 1357–1373, doi:10.1111/j.1365-2699.2006.01682.x.

Kozu, T., Iguchi, T., Shimomai, T., & Kashiwagi, N. (2009). Raindrop size distribution modeling from a statistical rain parameter relation and its application to the TRMM precipitation radar rain retrieval algorithm. *Journal of Applied Meteorology and Climatology*, *48*(4), 716-724.

Lavado Casimiro WS, Silvestre E, Pulache W (2010) Tendencias en los extremos de lluvias cerca a la ciudad del Cusco y su relación con las inundaciones de Enero del 2010. Extreme rainfall trends around Cusco and its relationship with the floods in January. Revista Peruana Geo-Atmosférica 2:89–98.

Lavado-Casimiro, W., & Espinoza, J. C. (2014). Impactos de El Niño y La Niña en las lluvias del Perú (1965-2007). Revista Brasileira de Meteorologia, v.29, n.2, 171 – 182.

Liu, C. (2011), Rainfall contributions from precipitation systems with different sizes, convective intensities, and durations over the tropics and subtropics, J. Hydrometeorol., 12(3), 394–412.

Lowman, L. E. L., and Barros, A. P. (2014). Investigating links between climate and orography in the Central Andes: coupling erosion and precipitation using a physical-statistical model. J. Geophys. Res. 119, 1322–1353. doi: 10.1002/2013JF002940

Marengo, J. A., W. R. Soares, C. Saulo, and M. Nicolini (2004), Climatology of the low-level jet east of the Andes as derived from the NCEP- NCAR reanalyses: Characteristics and temporal variability, J. Clim., 17(12), 2261–2280.

Peterson, T. C., & Vose, R. S. (1997). An overview of the Global Historical Climatology Network temperature database. Bulletin of the American Meteorological Society, 78(12), 2837–2849.

Martínez-Castro, D., Kumar, S., Flores Rojas, J. L., Moya-Álvarez, A., Valdivia-Prado, J. M., Villalobos-Puma, E., ... & Silva-Vidal, Y. (2019). The Impact of Microphysics Parameterization in the Simulation of Two Convective Rainfall Events over the Central Andes of Peru Using WRF-ARW. *Atmosphere*, *10*(8), 442.

Menne, M. J., Durre, I., Vose, R. S., Gleason, B. E., & Houston, T. G. (2012). An overview of the global historical climatology network-daily database. Journal of Atmospheric and Oceanic Technology, 29(7), 897–910.

Myers, N., R. A. Mittermeier, C. G. Mittermeier, G. A. Da Fonseca, and J. Kent (2000), Biodiversity hotspots for conservation priorities, Nature, 403(6772), 853–858.

Mohr, K. I., D. Slayback, and K. Yager (2014), Characteristics of precipitation features and annual rainfall during the TRMM era in the central Andes, J. Clim., 27(11), 3982–4001.

Moya-Álvarez, A., Gálvez, J., Holguín, A., Estevan, R., Kumar, S., Villalobos, E., ... & Silva, Y. (2018). Extreme rainfall forecast with the WRF-ARW model in the Central Andes of Peru. *Atmosphere*, *9*(9), 362.

Nesbitt, S. W., and A. M. Anders (2009), Very high resolution precipitation climatologies from the Tropical Rainfall Measuring Mission precipitation radar, Geophys. Res. Lett., 36, L15815, doi:10.1029/2009GL038026.

Rabatel A, Francou B, Soruco A, Gomez J, Cáceres B, Ceballos JL, Basantes R, Vuille M, Sicart JE, Huggel C, Scheel M, Lejeune Y, Arnaud Y, Collet M, Condom T, Consoli G, Favier V, Jomelli V, Galarraga R, Ginot P, Maisincho L, Mendoza J, Ménégoz M, Ramirez E, Ribstein P,

Rasmussen, K. L., M. M. Chaplin, M. D. Zuluaga, and R. A. Houze Jr. (2016), Contribution of extreme convective storms to rainfall in South America, J. Hydrometeorol., 17(1), 353–367, doi:10.1175/JHM-D-15-0067.1.

Romatschke, U., and R. A. Houze Jr. (2010), Extreme summer convection in South America, J. Clim., 23(14), 3761–3791, doi:10.1175/ 2010JCLI3465.1.

Saavedra, M. y Takahashi, K., 2017: Physical controls on frost events in the central Andes of Peru usingin situ observations and energy flux models. Agricultural and Forest Meteorology. Doi.org/10.1016/j.agrformet.2017.02.019

Stein, A.F., Draxler, R.R, Rolph, G.D., Stunder, B.J.B., Cohen, M.D., and Ngan, F., (2015). NOAA's HYSPLIT atmospheric transport and dispersion modeling system, Bull. Amer. Meteor. Soc., 96, 2059-2077, http://dx.doi.org/10.1175/BAMS-D-14-00110.1

Sun, X., and Barros, A. P. (2015a). Impact of Amazonian evapotranspiration on moisture transport and convection along the eastern flanks of the tropical Andes. Quart. J. R. Meteorol. Soc. 141, 3325–3343. doi: 10.1002/qj.2615

Tao, J., and A. P. Barros. “Prospects for flash flood forecasting in mountainous regions - An investigation of Tropical Storm Fay in the Southern Appalachians” Journal of Hydrology, 2013.

Takahashi, K., Montecinos, A., Goubanova, K., & Dewitte, B. (2011). ENSO regimes: Reinterpreting the canonical and Modoki El Niño. *Geophysical Research Letters*, *38*(10).

Takahashi, K., & Martínez, A. G. (2019). The very strong coastal El Niño in 1925 in the far-eastern Pacific. *Climate Dynamics*, *52*(12), 7389-7415.

Vera, C., et al. (2006a), The South American low-level jet experiment, Bull. Am. Meteorol. Soc., 87(1), 63–77, doi:10.1175/BAMS-87-1-63.

Vuille M, Francou B, Wagnon P, Juen I, Kaser G, Mark BG, Bradley RS (2008) Climate change and tropical Andean glaciers: past, present and future. Earth Sci Rev 89:79–96

Vuille M, Kaser G, Juen I. 2008. Glacier mass balance variability in the Cordillera Blanca, Peru and its relationship with climate and the large-scale circulation. *Global Planet. Change* **62**(1 – 2): 14 – 28. https://doi.org/10.1016/j.gloplacha.2007.11.003.

Wilson, A.M. and A.P. Barros, 2014: An Investigation of Warm Rainfall Microphysics in the Southern Appalachians: Orographic Enhancement via Low-Level Seeder–Feeder Interactions. J. Atmos. Sci., 71, 1783–1805, https://doi.org/10.1175/JAS-D-13-0228.1

Zubieta, R., Saavedra, M., Silva, Y., Giráldez, L., 2016: Spatial analysis and temporal trends of daily precipitation concentration in the Mantaro River basin: central Andes of Peru. Stochastic Environmental Research and Risk Assessment, 1-14, doi:10.1007/s00477-016-1235-5

Supplementary Figures

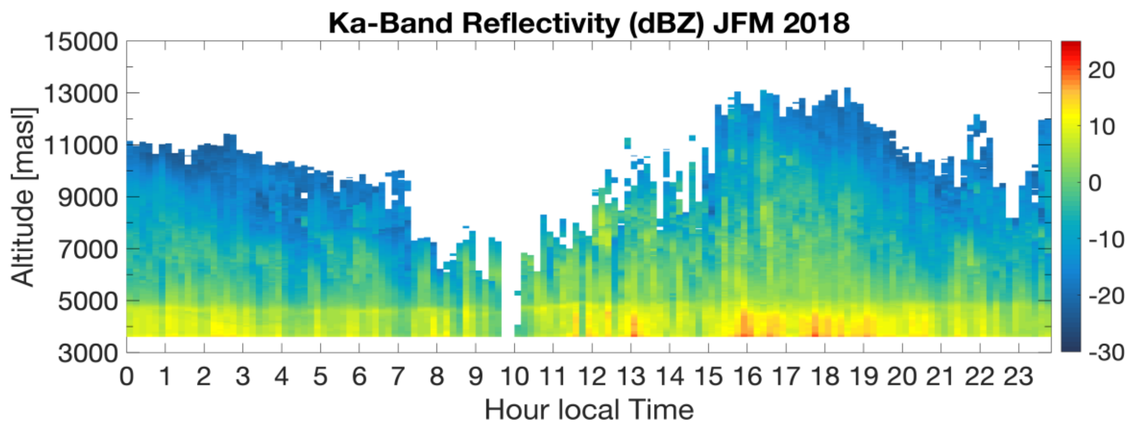

S1- Diurnal cycle of reflectivity vertical profiles and winds when rain is observed in the surface corresponding to JFM of 2018.

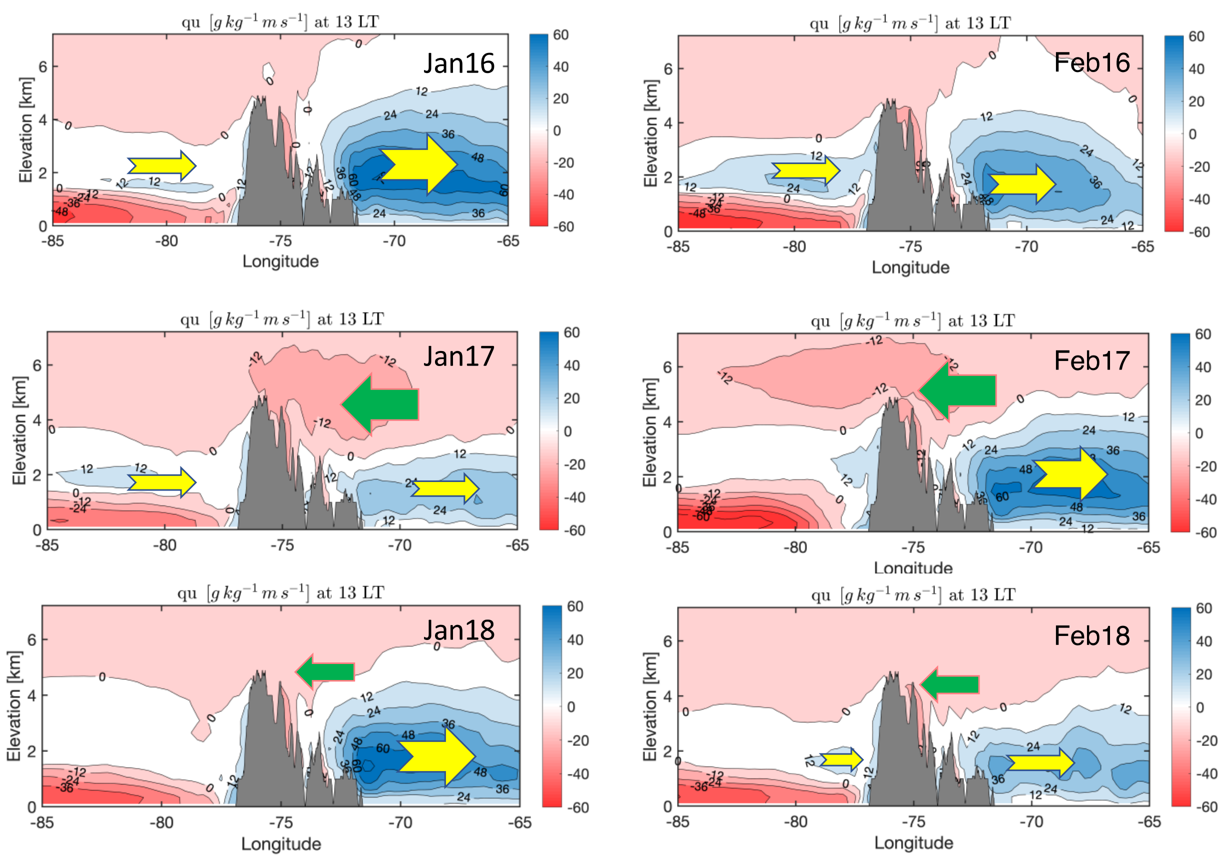

S2- Cross section at 12˚S of the East-West component of the moisture flux *uq* at 13 LT for January and February of 2016-2018. The arrows represent the direction to the east (yellow) and to the west (green) of *uq*, the size of the arrow represent the magnitude.